Spectrum of Engineering Sciences
ISSN (e) 3007-3138 (p) 3007-312X Volume 3, Issue 12, 2025

A NEW HYBRID SCHEME FOR TIKHONOV REGULARIZATION BASED MODEL FOR SIGNAL RESTORATION HAVING ADDITIVE NOISE

Shujaat Ali[1], Sobia Safder [2], Mushtaq Ahmad Khan[*3], Abdul Kabir[4], Muhammad Atif [5], Farhan Khan[6]

[1,*3,4,5,6]*University of Engineering and Technology, Mardan, 23200 Pakistan*
[2]*Department of Basic Sciences, Ripaha International University, Islamabad, Pakistan*

DOI: https://doi.org/10.5281/zenodo.18296065

Keywords

Article History
Received: 03 November 2025
Accepted: 17 December 2025
Published: 31 December 2025

Corresponding Author: *
Mushtaq Ahmad Khan

Abstract

Signal restoration plays an important role in signal processing and computer vision. In this article, we proposed a new Hybrid meshless scheme, which is the combination of a local meshless scheme and a domain decomposition method for signal restoration having additive Gaussian noise. These combined properties used in the proposed hybrid scheme divide the signal domain into local domains, which easily control the discontinuous jumps in derivatives in small domains and hence produce good restoration results as compared to other mesh-based and meshless schemes. The experimental results will demonstrate that the proposed hybrid scheme outperforms mesh-based and meshless schemes in terms of SNR values, computational times, and iterations required for convergence in image restoration.

1. Introduction

Signal processing is the process of converting or transforming data such that we can see things that are not visible to the human eye. Through signal processing, scientists and engineers can analyze, improve, and correct signals, including scientific data, audio streams, images, and video. The issue of signal de-noising has numerous applications in various technological and scientific domains, including communications, control, and machine learning. In literature, image noise can be categorized into two primary types: additive and multiplicative noise. This work focuses on the elimination of additive noise. The additive noise model is given as:

$$u = u_o + \lambda . \tag{1}$$

Where u is the given noisy signal is degraded by additive noise, and u_0 is the original signal. In literature, other techniques have been employed to address this issue, including wavelet techniques [1-3], adaptive smoothing [4, 5], stochastic schemes [6, 7], and anisotropic diffusion [8, 9].

Despite the known limitations of TV regularization, the Rudin–Osher–Fatemi (ROF) model effectively removes noise from signals and images while preserving important edge information.[10] However, due to its non-linear and non-differentiable nature, this approach also produces some undesirable effects, such as loss of signal contrast and increased computational cost [11–14]. This approach is commonly applied to the restoration of signals corrupted by additive noise [15]. Nevertheless, due to the non-linear and non-differentiable nature of the associated partial differential equation, the model suffers from several limitations that can introduce undesirable artifacts and signal degradation [16, 17].

One of the most well-known techniques for signal de-noising is based on the TV known as Tikhonov regularization based model [18]. Recently, variational methods have been employed to address difficulties

related to TV models, yielding successful restoration outcomes, as demonstrated in previous studies [19–20]. In traditional variational methods, the PDE is derived from the minimization functional that incorporates additive noise. This approach is employed to achieve a smooth solution for signal de-noising. However, the equation of the EL-PDE when connected to a TV model is invariably a non-linear and non-differentiable PDE. Consequently, the traditional numerical methods were unable to effectively solve the EL-PDE for obtaining a smooth numerical solution, resulting in the loss of fine details in the signal de-noising process. Additionally, Tikhonov regularization has been adapted to include total variation regularization, which is particularly effective for maintaining edges in images [21]. By effectively balancing the trade-off between noise reduction and detail preservation. Overall, this approach addresses the challenges associated with ill-posed problems, making it a foundational method in the field.

In the 1970s, Radial Basis Function (RBF) methods emerged to enhance the structural stability of numerical schemes, particularly suited for handling scattered data points [22]. This flexibility allows the shape of the computational domain to be dictated by application needs rather than by the limitations of numerical methods. Recently, RBF techniques have gained traction in both approximation theory and the numerical resolution of partial differential equations (PDEs), with the RBF interpolation method, or Collocation method, being the most prevalent [23-25]. The appeal of RBF methods lies in their meshless nature, which requires only a discrete set of points to represent continuous problems, offering greater efficiency compared to traditional techniques like Finite Difference Methods (FDM), pseudo-spectral methods, and Finite Element Methods (FEM).

RBF techniques can be implemented in two main frameworks: Global and Local Meshless Methods. The Global Meshless Method is effective for solving PDEs with smooth solutions due to its adaptive and computational properties. However, its reliance on full matrices during discretization can lead to ill-conditioning issues. To mitigate the sensitivity of shape parameters and these ill-conditioning problems, the Local Meshless Scheme (LMS) was introduced. Initially proposed for diffusion problems, LMS has shown notable improvements in both accuracy and computational efficiency through its localized structure and adaptive approach. The LMS has been extensively applied across various fields in engineering and science due to its practicality. This method reduces the complexity of the collocation matrix by solving several smaller matrices that correspond to overlapping influence sub-domains, where each matrix is defined by the number of nodes in each node's influence area. Motivated by the advantages of the LMS, we propose applying it to approximate solutions for EL-PDEs related to the Rudin-Osher-Fatemi (ROF) model, targeting effective additive noise removal from signals. This approach promises to enhance noise reduction efficiency and speed, capitalizing on the beneficial properties of the LMS [26].

The Domain Decomposition Scheme utilizing local Radial Basis Function (RBF) methods is an effective strategy for solving partial differential equations (PDEs) by partitioning a computational domain into smaller subdomains. This approach allows each subdomain to be addressed independently, facilitating parallel computation and improving resource efficiency [27]. Within these subdomains, local RBFs are employed for interpolation and approximation, offering high accuracy and the advantage of being meshless, meaning they do not rely on a structured grid [28]. To maintain continuity and compatibility across the boundaries of subdomains, specific coupling conditions are implemented, ensuring that solutions from adjacent subdomains align properly [29]. By concentrating on local RBFs, this method effectively captures complex behaviors in the solution while preserving computational efficiency [30]. The independence of subdomains also lends itself to parallel processing, significantly accelerating computation, especially in large-scale or high-dimensional PDE scenarios [31]. This methodology finds extensive applications in diverse fields such as fluid dynamics, structural analysis, and heat transfer, where solving intricate PDEs is crucial [32]. Moreover, the approach has demonstrated strong convergence properties and stability, making it a dependable option for practical applications [33].

In this paper, we will focus on Signal restoring images using the Tikhonov model for partial differential equations (PDEs). Our approach involves employing Domain Decomposition techniques in conjunction with

Local Radial Basis Functions. This combination aims to enhance the effectiveness of the image restoration process. By leveraging the strengths of both methods, we seek to achieve improved results. Ultimately, our goal is to develop a robust framework for signal image restoration.

2. Literature Review

2.1 Tikhonov regularization Model:

Tikhonov regularization serves as a fundamental approach for image restoration, differentiating itself through its use of the gradient-based energy functional. Overall, this method provides a robust framework for improving image quality. The distinction between L2 and L1 norms highlights different approaches to handling image data [18].

$$\min_u \{E(u)\} = \min_u \int_\Omega |\nabla u(x,y)|^2 d\Omega + \lambda \int_\Omega (u-u_0)^2 d\Omega. \tag{2}$$

Forward finite difference method. The resulting PDE is given below.

$$\frac{\partial u}{\partial t} = \left(u_{xx} + u_{yy}\right) - \lambda\left(u - u_0\right). \tag{3}$$

Tikhonov regularization provides strong smoothing effects; however, it struggles to preserve key geometric features in images, such as edges, corners, and textures. This challenge stems from the method's focus on achieving smoothness, which can compromise sharp details. Consequently, although Tikhonov regularization is beneficial for noise reduction, it may not be the best choice for tasks requiring the retention of intricate features. In such cases, other techniques might be necessary to maintain these important attributes [19-20].

2.2 Local Kansa Method/local RBF

In this section, we focus on the local Radial Basis Function (RBF) method. The local RBF technique builds the approximation in a neighborhood, using only a limited number of nodes close to each evaluation point [34, 35]. Formally, an RBF is defined as a function that depends solely on the distance from the origin, i.e., $\phi(x) = \phi(|x|)$. More generally, with a fixed center C, the function is expressed as $\phi(x, C) = \phi(|x - C|)$ where the center point and its surrounding stencil are used for computation over P and x_p. Any function ϕ that satisfies the condition $\phi(x) = \phi(\|x\|)$ is considered a radial basis function, with the norm always taken as the Euclidean distance. If n is odd, there are exactly n center points, while if n is even, there will be n+1 center points. This distinction ensures that local approximations are made effectively by adjusting the number of center points according to the stencil size. A radial basis function (RBF) is a real-valued function that depends on the distance from the origin, specifically characterized by the property that the norm is always based on Euclidean distance. This forms the basis for RBF interpolation.

$$T\left(y_1\right) = \sum_{i=1}^{N} \alpha_j \phi_j \left(\left\| y_i^c - y_j^c \right\|_2\right) \text{ for } i, j = 1, 2, 3, \ldots\ldots N, \tag{4}$$

$$B = \begin{bmatrix} \phi\left(\left\|y_1^c - y_1^c\right\|\right)_2 & \phi\left(\left\|y_1^c - y_2^c\right\|\right)_2 & \ldots\ldots & \phi\left(\left\|y_1^c - y_N^c\right\|\right)_2 \\ \phi\left(\left\|y_2^c - y_1^c\right\|\right)_2 & \phi\left(\left\|y_2^c - y_2^c\right\|\right)_2 & \ldots\ldots & \phi\left(\left\|y_2^c - y_N^c\right\|\right)_2 \\ \phi\left(\left\|y_3^c - y_1^c\right\|\right)_2 & \phi\left(\left\|y_3^c - y_2^c\right\|\right)_2 & \ldots\ldots & \phi\left(\left\|y_3^c - y_N^c\right\|\right)_2 \\ \vdots & \vdots & \vdots & \vdots \\ \phi\left(\left\|y_N^c - y_1^c\right\|\right)_2 & \phi\left(\left\|y_N^c - y_2^c\right\|\right)_2 & \ldots\ldots & \phi\left(\left\|y_N^c - y_N^c\right\|\right)_2 \end{bmatrix} \tag{5}$$

$$B\alpha = f \tag{6}$$

$$\alpha = B^{-1} f \tag{7}$$

Where $\alpha = (\alpha_1, \alpha_2, \alpha_3 ..... \alpha_N)^t$, $f = (f(\theta_1), f(\theta_2), f(\theta_3) ..... f(\theta_N))^t$ and $B = \left[\phi_{ij}\right] = B_{ij} \in R^{N \times N}$

$$B = \left[\phi_{ij}\right] = \phi\left(\theta_i - \theta_j\right), i, j = 1, 2, 3 ..... N \text{ with } \phi_{ij} = \phi_{ji} \text{s} \tag{8}$$

where matrix B is known as the interpolation system matrix. Now for "N" centers points and 'K' evaluation points using again the RBF interpolation condition, we have

When dealing with N center points and k evaluation points, the Radial Basis Function (RBF) interpolation condition is reapplied to define the connection between them. This guarantees that the interpolation accurately reflects the behavior of the target function at the chosen evaluation points. The RBF scheme is

$$T(y_1) = \sum_{i=1}^{K} \alpha_j \phi_j \left(\left\| y_i - y_j^c \right\|_2 \right) \text{ for } i, j = 1, 2, 3, ...N \text{ and } j = 1, 2, 3, \ldots \ldots \ldots N \tag{9}$$

Where $\alpha = B^{-1} f$ (10)

and

$$H = \begin{bmatrix} \phi\left(\left\|y_1 - y_1^c\right\|\right)_2 & \phi\left(\left\|y_1 - y_2^c\right\|\right)_2 & ..... & \phi\left(\left\|y_1 - y_N^c\right\|\right)_2 \\ \phi\left(\left\|y_2 - y_1^c\right\|\right)_2 & \phi\left(\left\|y_2 - y_2^c\right\|\right)_2 & ..... & \phi\left(\left\|y_2 - y_N^c\right\|\right)_2 \\ \phi\left(\left\|y_3 - y_1^c\right\|\right)_2 & \phi\left(\left\|y_3 - y_2^c\right\|\right)_2 & ..... & \phi\left(\left\|y_3 - y_N^c\right\|\right)_2 \\ \vdots & \vdots & \vdots & \vdots \\ \phi\left(\left\|y_k - y_1^c\right\|\right)_2 & \phi\left(\left\|y_k - y_2^c\right\|\right)_2 & ..... & \phi\left(\left\|y_k - y_N^c\right\|\right)_2 \end{bmatrix} \tag{11}$$

And H is $K \times N$ matrix is called evaluation matrix. Also $\alpha = (\alpha_1, \alpha_2, ..., \alpha_k)^t$ and $\omega = (\omega(y_1), \omega(y_2), ..., \omega(y_n))^t$, are the $N \times 1$ matrices. Hence

$$\omega = H\alpha. \tag{12}$$

Put the value of α from (10) in (12)

$$\omega = HB^{-1} \text{f}. \tag{13}$$

Let $HB^{-1} = D.$ (14)

$$\omega = Df, \tag{15}$$

Equation (15) $N \times 1$ system and is called the approximation solution of the function $\omega(y_i)$ and given points $y_i \;\; i = 1, 2, ..., N$. For more information [25].

2.3 Domain Decomposition Method (DDM):

Domain Decomposition Methods (DDM) are numerical techniques that divide a computational domain into smaller subdomains to tackle large-scale problems effectively. These methods are particularly advantageous for solving partial differential equations (PDEs) and are designed to make optimal use of parallel computing environments. DDM can be categorized into two main types: overlapping and non-overlapping methods. Each category offers distinct mathematical frameworks and methodologies for addressing various challenges [27, 28].

By partitioning a computational domain into smaller subdomains, Domain Decomposition Methods (DDM) are employed to manage large-scale issues efficiently. These techniques are particularly useful for solving partial differential equations (PDEs) and are specifically adapted to leverage parallel computing capabilities.

DDM approaches can be classified into two broad categories: overlapping and non-overlapping. Each approach provides unique mathematical structures and strategies for solving problems, allowing for flexibility in application depending on the specific needs of the problem [29-33].

2.3.1 Partitioning the domain:

The domain Ω is divided into two non-overlapping subdomains.

$$\Omega = \bigcup_{i=1}^{2} \Omega_i \tag{16}$$

With $\Omega_1 \bigcap \Omega_2 = \phi$ and $\Omega_1 \bigcup \Omega_2 = \Omega$

2.3.2 Local problem formulation:

Within each subdomain Ω_i, the PDE is solved locally. For example, consider the Tikhonov model PDE:

$$\frac{\partial u}{\partial t} = \left(u_{xx} + u_{yy}\right) - \lambda\left(u - u_0\right) \quad , \Omega_i \quad \text{for } i = 1,2 \tag{17}$$

2.3.3 Interface conditions:

At the interface between sub-domains, the continuity of the solution and the flux is enforced for Ω_1 and Ω_2. This typically involves:

$$\frac{\partial u_1}{\partial t} = \left(u_{1xx} + u_{1yy}\right) - \lambda\left(u_1 - f_0\right) \quad \Omega_1. \tag{18}$$

$$\frac{\partial u_2}{\partial t} = \left(u_{2xx} + u_{2yy}\right) - \lambda\left(u_2 - f_0\right) \quad \Omega_2. \tag{19}$$

$$u_1(x) = u_2(x) \quad \text{on } \Gamma_{12}. \tag{20}$$

Where Γ_{12} denote the interface between Ω_1 and Ω_2, and n is the unit normal vector on Γ_{12}.

3. Proposed Hybrid Meshless Algorithm (M2)

In this section, we introduce an algorithm, using both Local Radial Basis Function interpolation and Domain Decomposition Method to solve the Tickonov model PDE (1).

Suppose $\{x_i\}_{i=1}^{N}$ is the N distinct evaluation points in the domain Ω. The following equation is true for any radial basis function, $\varphi(r) = \|r\|_2$ in R. For N center points $\{x_{c_j}\}_{j=1}^{N}$, we have

$$u(p) = \sum_{j=1}^{N} \alpha_j \varphi\left(\left\| p - p_{c_j} \right\|_2\right) \tag{21}$$

Where αj represents the coefficient of RBF and is given by

$$S(p_i) = f_0 \tag{22}$$

Is the set of points that usually coincides with the centres.

$$H\alpha = f_0 \tag{23}$$

Where $\alpha = (\alpha_1, \alpha_2, \alpha_3 \ldots\ldots \alpha_N)^t$, is unknown and $u_0 = \left(u_{01}, u_{02}, u_{03} \ldots\ldots u_{0N_c}\right)^t$ is known are $N_c \times 1$ matrix.

The matrix H is called the interpolation matrix, and is given by

$$H = \left[\varphi_{ij}\right] = \left[\left(\left\| x_i - x_{c_j} \right\|\right)\right]_{1 \le i, j \le N_c} \tag{24}$$

This matrix H is always invertible because it is always a positive definite matrix.
And hence we have

$$\alpha = H^{-1}u_0 \tag{25}$$

Where α is $N_c \times 1$ a matrix. This interpolation matrix is evaluated using equation (21) at N evaluation points $\{x_i\}_{i=1}^{N}$ from which to form the evaluation matrix 'K' that is

$K = \left[\varphi_{ij}\right] = \left[\left(\left\|x_i - x_{c_j}\right\|\right)\right]$ for i=1, 2, 3.....N and j= 1, 2, 3.....Nc.

$$u = K\alpha \tag{26}$$

Now using equation [25] in equation [26], we get

$$u = KH^{-1}u_0 \tag{27}$$

Or

$$u = Du_0 \quad \text{where} \quad D = KH^{-1} \tag{28}$$

Which gives the approximate solution at any point in the domain Ω is $N_c \times 1$ matrix.

The equation (17) is rewritten as follows.

$$\frac{\partial u_1}{\partial t} = \left(u_{1xx} + u_{1yy}\right) - \lambda\left(u_1 - f_0\right) \quad , \Omega_i \tag{29}$$

The semi-implicit gradient descent method is applied to (29).

$$\frac{u_1^{(k+1)} - u_1^{(k)}}{\partial t} = \left(\left((u_1)_{xx}\right)^{(k)} + \left((u_1)_{yy}\right)^{(k)}\right) - \lambda\left(u_1^{(k)} - \left(f_0\right)^{(0)}\right) \tag{30}$$

Put equation (28) in equation (30), and we will get a linear resultant equation.

$$G(u_1^{\,k})u_1^{\,k+1} = G(u_1^{\,k})u_1^{\,k} + dt\left(\left((u_1)_{xx}\right)^{(k)} + (u_1)_{yy}^{(k)}\right) - G(u_1^{\,k})dt\lambda\left(u_1^{(k)} - \left(f_0\right)^{(0)}\right) \tag{31}$$

Where $G(u_1) = ((u_1^k)_x + (u_1^k)_y)^{\frac{1}{2}}, (u_1)_{xx} = (\omega_1)_{xx}\,\mathrm{f}_0, (u_1)_{yy} = (\omega_1)_{yy}\,\mathrm{f}_0, \mathrm{f}_0^0 = f_0$

Similarly, we can solve for equation (18). i-e

$$G(u_2^{\,k})u_2^{\,k+1} = G(u_2^{\,k})u_2^{\,k} + dt\left(\left((u_2)_{xx}\right)^{(k)} + \left((u_2)_{yy}\right)^{(k)}\right) - G(u_2^{\,k})dt\lambda\left(u_2^{(k)} - \left(f_0\right)^{(0)}\right) \tag{32}$$

Where $G(u_2) = (u_2^k)_x + u_2^k)_y)^{\frac{1}{2}}, (u_2)_{xx} = (\omega_2)_{xx}\,\mathrm{f}_0, (u_2)_{yy} = (\omega_2)_{yy}\,\mathrm{f}_0, \mathrm{f}_0^0 = f_0$

In the Kansa method, the RBF used in the collocation technique provides flexibility in choosing the RBF, with the Multiquadric (MQ) function being the most popular due to its spectral accuracy when the shape parameter is properly selected. In the M2 scheme, the shape parameter c and regularization parameters β1 and β2 are adjusted based on the size and noise level of the image being analyzed. The collocation approach applied to the Euler-Lagrange Equation (32) results in a novel solution because of the MQ-RBF interpolation, which helps preserve image edges. Additionally, the weighted mean derived from the interpolation process smooths the solution to Equation (32), with the smoothness depending on the Euclidean distance between noisy and non-noisy pixels. This leads to effective image reconstruction, reducing the staircase effect often seen in image processing.

Algorithm 1: Algorithm for the Proposed Hybrid Meshless Scheme (M2)

RBF Interpolation:

1. Choose $N = N_c$, n number of data pixel points.
2. Calculate "α" according to the Eq. (25) by MQ-RBF.
3. Compute u by using Eq. (28) by MQ-RBF.

Tickonov regularization:

4. Pick out the values for β1, β2,s and f.
5. Introduce n Nc number of data pixel centers i.e., $x_{c_1} \le x_{c_2} \le \ldots\ldots\ldots x_{c_n}$ next choose n = 0.
6. Replace u as MQ-RBF utilizing Eq. (28) in Eq. (32).
7. Choose $n = n+1$, for each data center point xci, for $1 \le i \le N$, then compute u^{n+1} according to the Eq. (32) by Kansa method (collocation scheme). Where $f^0 = f$
8. $\dfrac{\left\|u^{n+1} - u^n\right\|}{\left\|u^n\right\|} \le \in$ Formula is used to break the iterative process, move to Step (10).
9. Turn to Step (7).
10. End.
11. Output result u_1
11. Similarly we will find u2 as done for u1 for the solution of equation (20)
11. Hence Output result $u = u_1 + u_2$

4. Results and Discussions:

This section presents experimental results and analyses conducted on various real signals to evaluate the performance of the proposed meshless algorithm M2. Noisy signals are used to assess the performance of both M1 and M2. The test signals, which include salt-and-pepper noise (variation), are shown in the figure. In this study, we compare the restoration outcomes of the proposed M2 with those of the traditional mesh-based method M1 to assess the signal recovery performance.

We chose the unique size of $N = N_c$size and used the suggested meshless techniques M2. The SNR values is taken to consider to quantify the denoising image. The measure is widely used for the quantity of restoring single.

SNR is defined as:

$$SNR = 10 \times \log_{10} \frac{\left\|\omega - \omega_0\right\|}{\left\|n - n_0\right\|} \tag{29}$$

Where ω_0 represent the final de-noise signal and $(\mathrm{M} \times N)$ represent the single data size of the image, and ω represent the provided original signal. The restoration performance depends upon the value of SNR. (i-e greater the SNR value result the greater the restoration performance.)

$$\frac{\left\|\omega^{(n+1)} - \omega^{(n)}\right\|}{\left\|\omega^{(n)}\right\|} \le \in \tag{30}$$

Where ∈ denotes the highest acceptable level of accuracy. Here it is set to be 10^{-1}. In this paper, we implement the MQ-RBF method to evaluate and compare the outcomes of the $M2$ and $M1$ schemes. The MQ_RBF is defined for each point (u_i, u_j) as follows:

$$\phi_j(u,v) = \sqrt{c^2 + \omega_j^2} = \sqrt{c^2 + \left((u-u_j)^2 + (v-v_j)^2\right)} \tag{31}$$

Inverse multi-quadric (IMQ-RBF) is as follows

$$\phi_j(u,v) = \frac{1}{\sqrt{c^2 + \omega_j^2}} = \frac{1}{\sqrt{c^2 + \left((u-u_j)^2 + (\mathrm{v}-\mathrm{v}_j)^2\right)}} \tag{32}$$

Also, the Gaussian (GA) RBF is

$$\phi_j(u,v) = e^{-c^2\omega^2} = e^{-c^2[(u-u_j)^2 + (v-v_j)^2]} \tag{33}$$

Where

$$\omega = \sqrt{[(u-u_j)^2 + (v-v_j)^2]}$$

Analysis 1:

In this comparison, 70th, 120th and 200th lines taken from Lena image are compared for signal restoration having additive Gaussian noise with noise levels of 30%, 35%, and 45%, respectively, for the proposed hybrid meshless scheme M2 and mesh-based method M1. The noisy and original signal comparison for 30%, 38%, and 45%, respectively, is given in Figures 1(a), 2(a), and 3(a) regarding the signals and histogram comparison. It can be seen that the image restoration regarding signals and histogram comparisons of proposed scheme M2 far better than M1 due to the MQ-BRF used in meshless method along with domain decomposition method used in M2 which is not only responsible to denoised the signals (signal denoising and histogram) because of the domain decomposition method property that divide the signal domain into two domains which is responsible to control the discontinuities in the small domains and hence denoised the signals better than mesh-based M1. These results are given in Figures 1(b), 2(b) and 3(b) for M1 and Figures 1(c), 2(c) and 3(c) for M2, respectively. It can also be seen from Table 1 that the SNR values of the proposed method M2 are greater than M1which shows the better signal restoration of M2 over M1. Table 1 also shows that the CUP time and number of iterations of M2 are less than M1, which indicates the quick restoration performance of M2 over M1.

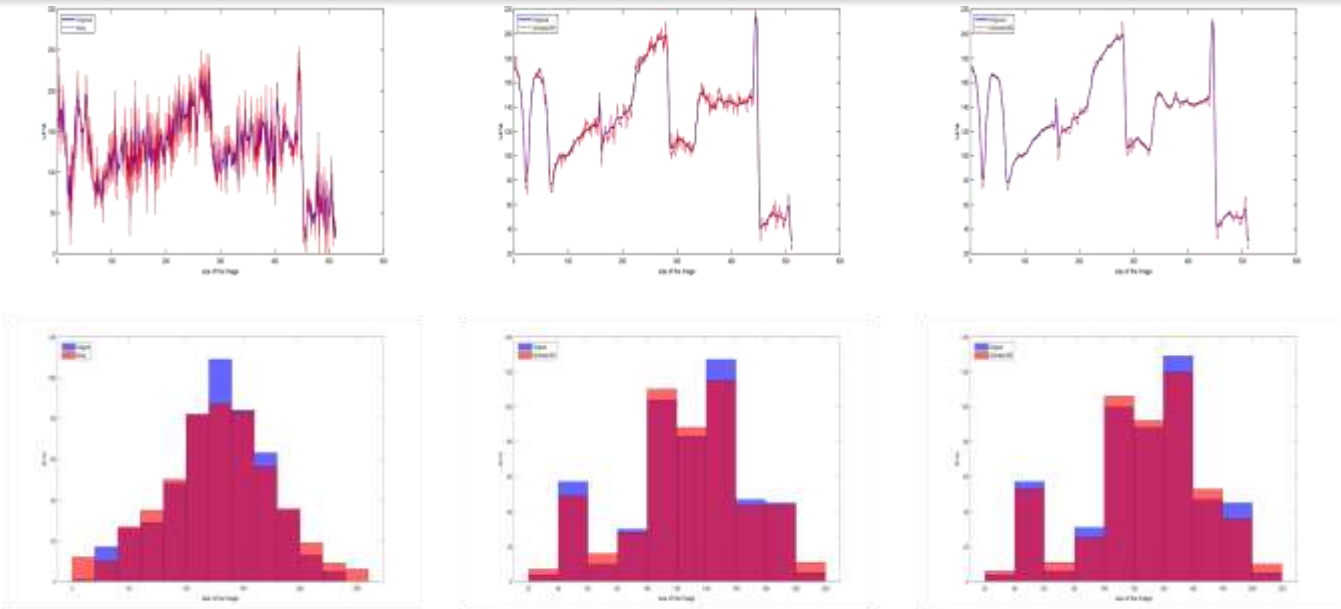

(a) True and Noisy signals along with histogram (b) True and M1 signals along with histogram (c) True and M2 signals along with histogram

Figure 1: Comparison 70th signal taken from Lena Image for signal restoration: (a) True and Noisy signals associated with a histogram having a noise level is 30%; (b) True and restored signals associated with a histogram by M1; (c) True and restored signals associated with a histogram by M2. The true signal is denoted by blue color, while noisy and restored signals are denoted by red colors.

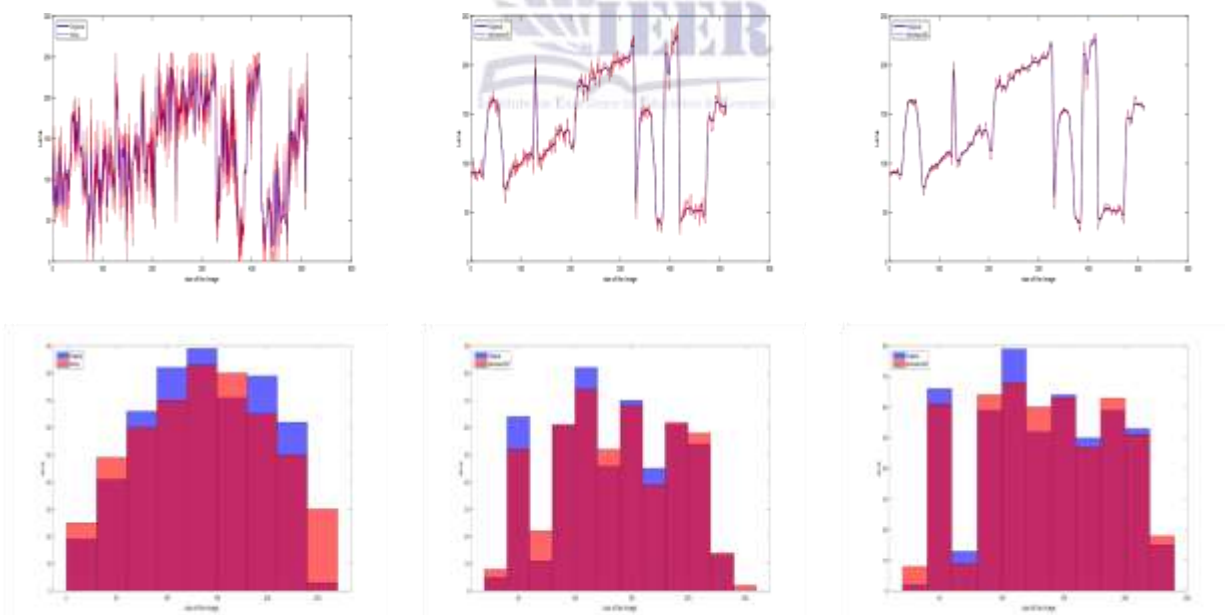

(a) Ture and Noisy signals along with histogram (b) True and M1 signals along with histogram (c) True and M2 signals along with histogram

Figure 2: Comparison 120th signal taken from Lena Image for signal denoising: (a) Actual and Noisy signals Connected with histogram having noise level is 37%; (b) Actual and denoised signals connected with histogram by M1; (c) Actual and denoised signals connected with histogram by M2. The actual signal is denoted by blue color while noisy and denoised signals are denoted by red colors.

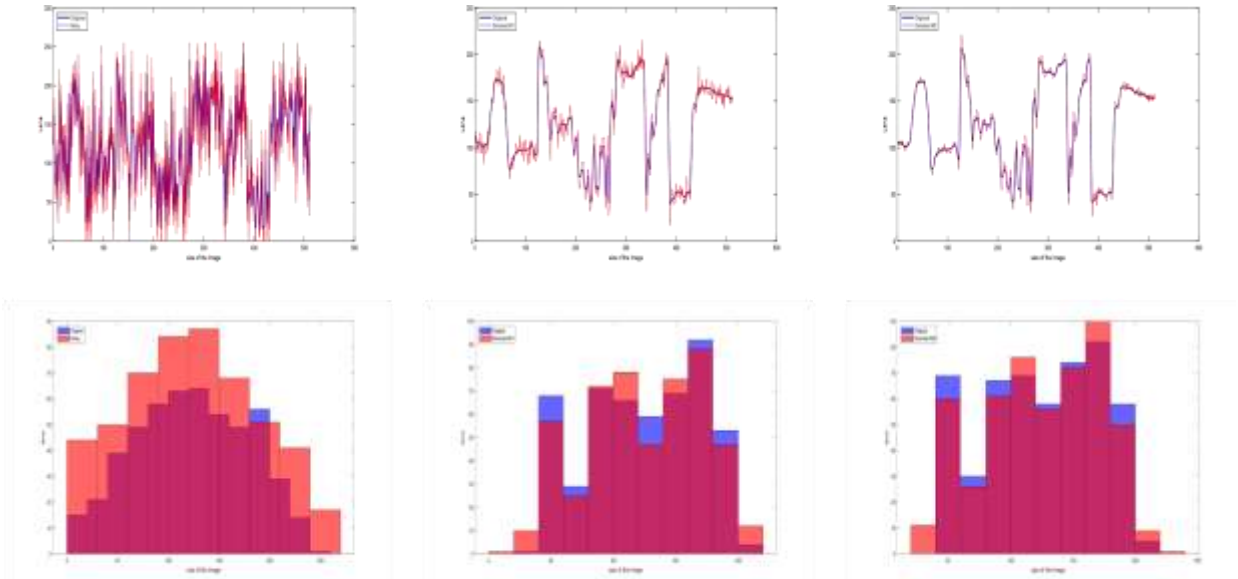

(a) True and Noisy signals along with histogram (b) True and by M1 signals along with histogram (c) True and by M2 signals along with histogram

Figure 3: Comparison 200th signal taken from Lena Image for signal reconstruction: (a) Actual and Noisy signals connected with a histogram containing noise level is 45%; (b) Actual and reconstructed signals connected with a histogram by M1; (c) Actual and reconstructed signals connected with a histogram by M2. The actual signal is reconstructed by blue color while noisy and reconstructed signals are denoted by red colors.

Table 1: SNR values and computational time (iterations and time in seconds) comparison between M1 and M2.

S. No	Signal selected from the Lena	Size	M1			M2		
			SNR	Time (s)	Iterations	SNR	Time (s)	Iterations
1	70th	512^2	24.11	14	22	24.27	9	16
2	120th	512^2	23.90	18	27	24.47	12	20
3	200th	512^2	23.60	22	32	23.91	18	27

4.1 Local Meshless Scheme for Total Variation Based L1 Model for Signal Restoration Model Connected with Additive Noise (M3)

Tawab. et. al [23] proposed a Local meshless scheme for the numerical solution of the TV-based L1 model for signal restoration. The TV-L1 model is given as under.

$$W = \min_{w}\{E(w)\}\int_{\Omega}\left|\nabla w(x,y)\right|d\Omega + \lambda\int_{\Omega}\left|w-w_o\right|d\Omega \tag{34}$$

where w_o is the given noisy image, w is the denoised image and $\lambda$is a regularization parameter. The associated time-dependent EL-PDE associated with model (34) is given as under.

$$\frac{\partial w}{\partial t} = \frac{w_{xx}w_y^2 - 2w_x w_y w_{xy} + w_{yy}w_x^2}{\left(w_x^2 + w_y^2\right)^{\frac{3}{2}}} - \lambda\frac{\left(w-w_o\right)}{\left|w-w_o\right|}. \tag{35}$$

Using the Local Meshless scheme, by the gradient descent method, the time-dependent EL-PDE is given as under.

$$L\left(w^{(n)}\right)w^{(n+1)} = L\left(w^{(n)}\right)w^{(n)} + dt\left[\left(w_{xx}^{(n)} + w_{yy}^{(n)}\right)\left(\left(w_x^2\right)^{(n)} + \left(w_y^2\right)^{(n)}\right) - \left(2w_x^{(n)}w_y^{(n)}\left(w_x^{(n)}w_y + w_x w_y^{(n)}\right) + w_x^2 w_{xx}^{(n)} + w_y^2 w_{yy}^{(n)}\right)\right] -$$

$$dt\left[L\left(w^{(n)}\right)\lambda\frac{\left(w^{(n)} - w^{(0)}{}_o\right)}{\left|w^{(n)} - w^{(0)}{}_o\right|}\right], \quad t > 0, \quad (x, y) \in R. \tag{36}$$

Where $L(w) = \left(w_x^2 + w_y^2\right)^{\frac{3}{2}}, w_x = Hw_o, w_{xx} = H_{xx}w_o, w_y = H_y w_o, w_{yy} = H_{yy}w_o, \frac{\partial w}{\partial n} = w_n = H_n w_o$ and $w^{(0)} = w_o$. For more information, see [23].

Analysis 2:

In this second analysis, signals 170th and 220th taken from cameraman image are compared for two methods that are M2 (proposed hybrid method) and M3 (meshless method) for signal denoised having additive noise with noise levels 45% and 50%. The noisy and original signals in terms of signals and histogram are given in Figures 4(a) and 5(a). We noticed that both schemes M2 and M3 are meshless scheme containing MQ-RBF but the signal restoration of M2 is better than M3 because of the domain decomposition property involved in M3. This property is capable to divide the domain in to two local domains which has the property to control the discontinuity of the derivatives inside the local domain of the signal and hence produce good restoration result compared to M3 which has larger domain because of its global meshless property. The restored signals and their respective hoistrooms of M2 and M3 are shown in Figures 4(b), 5(b) and 4(c), 5(c), respectively. It can also be seen from Table 2 that SNR values of M2 are greater than M3 which shows the good restoration performance of M2 over M3. Also, Table 2 indicate that the restoration performance regarding computational time and iteration required for restoration of M2 are less than M3 which shows the quick restoration performance of M2 over M3.

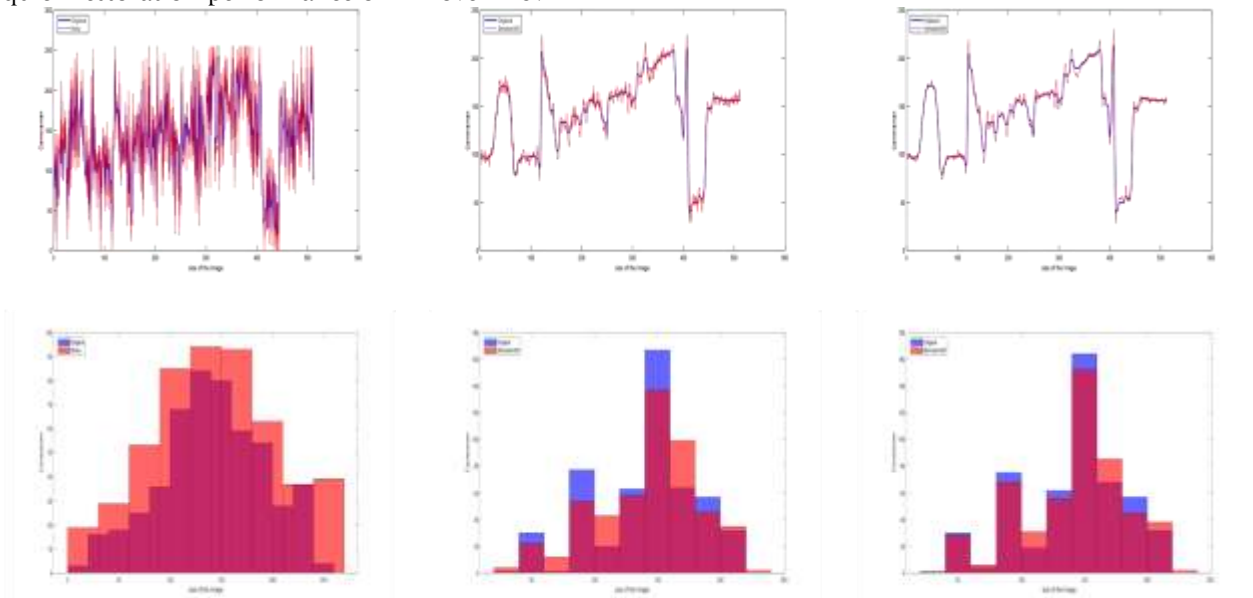

(a) **True and Noisy signals along with histogram** (b) **True and M3 signals along with histogram** (c) **True and M2 signals along with histogram**

Figure 4: Comparison 170th signal taken from Cameraman for signal denoising: (a) Actual and degraded signals associated with histogram having noise level is 45%; (b) Actual and denoised signals associated with histogram by M3; (c) Actual and denoised signals associated with histogram by M2. The actual signal is denoted by blue color while noisy and denoised signals are denoted by red colors.

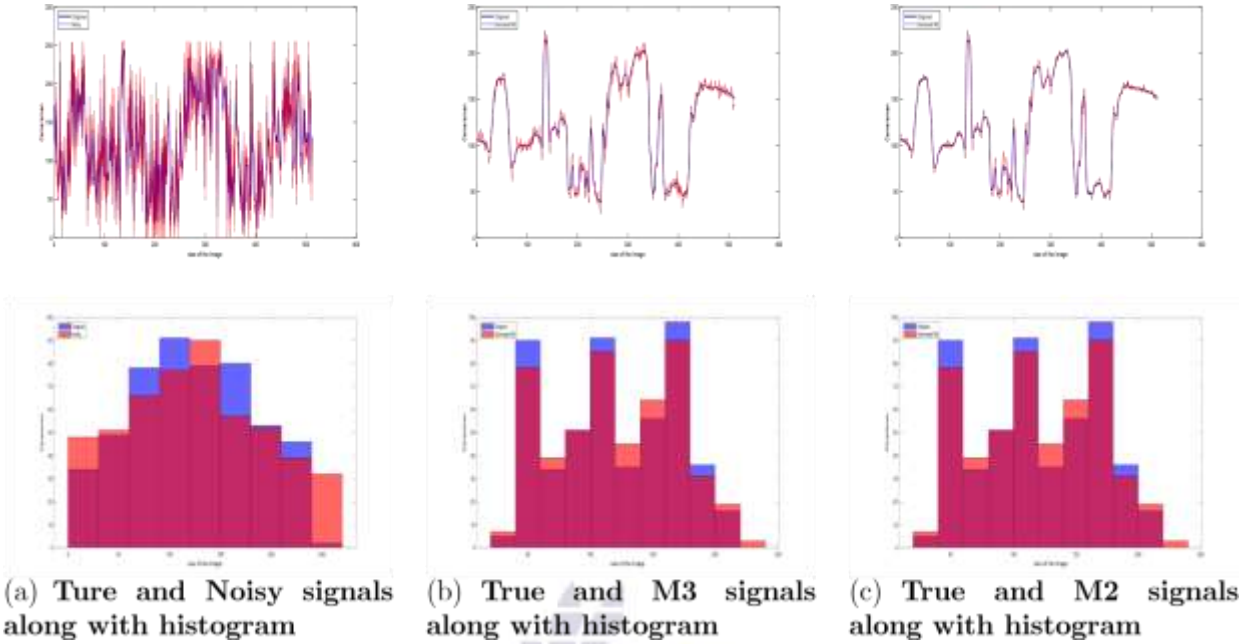

(a) Ture and Noisy signals along with histogram (b) True and M3 signals along with histogram (c) True and M2 signals along with histogram

Figure 5: Comparison 220th signal taken from Cameraman for signal denoising: (a) Ture and degraded signals connected with histogram having noise level is 50%; (b) Ture and denoised signals connected with histogram by M3; (c) Ture and denoised signals connected with histogram by M2. The actual signal is denoted by blue color while noisy and denoised signals are denoted by red colors.

Table 2: Comparison of methods M3 and M2 regarding SNR values and computational time (iterations and time in seconds).

S.No	Signal selected from the Cameraman	Size	M3			M2		
			SNR	Time (s)	Iterations	SNR	Time (s)	Iterations
1	170th	512^2	23.01	15	21	23.17	12	17
2	220th	512^2	22.91	18	25	23.05	14	22

Analysis 3:

In this analysis, M1 is compared with the proposed method M2 for the associated three bases functions, i.e., MQ-RBF, IMQ-RBF, and GA-RBF, for signal restoration having additive noise 50%. The 110th signal taken from Lena image is tested in this analysis. Figures 6 and Table 3 indicate that the signal restoration regarding signals and associated histogram along the computational time and iterations required for convergence of proposed M2 is far better that of M1 due to its meshless applications discussed in anaysis1. Furthermore, the signal restoration and associated histogram of M2 for MQ-RBF is better than both IMQ-RBF and GA-RBF, which proves the Hardy claim [aaa].

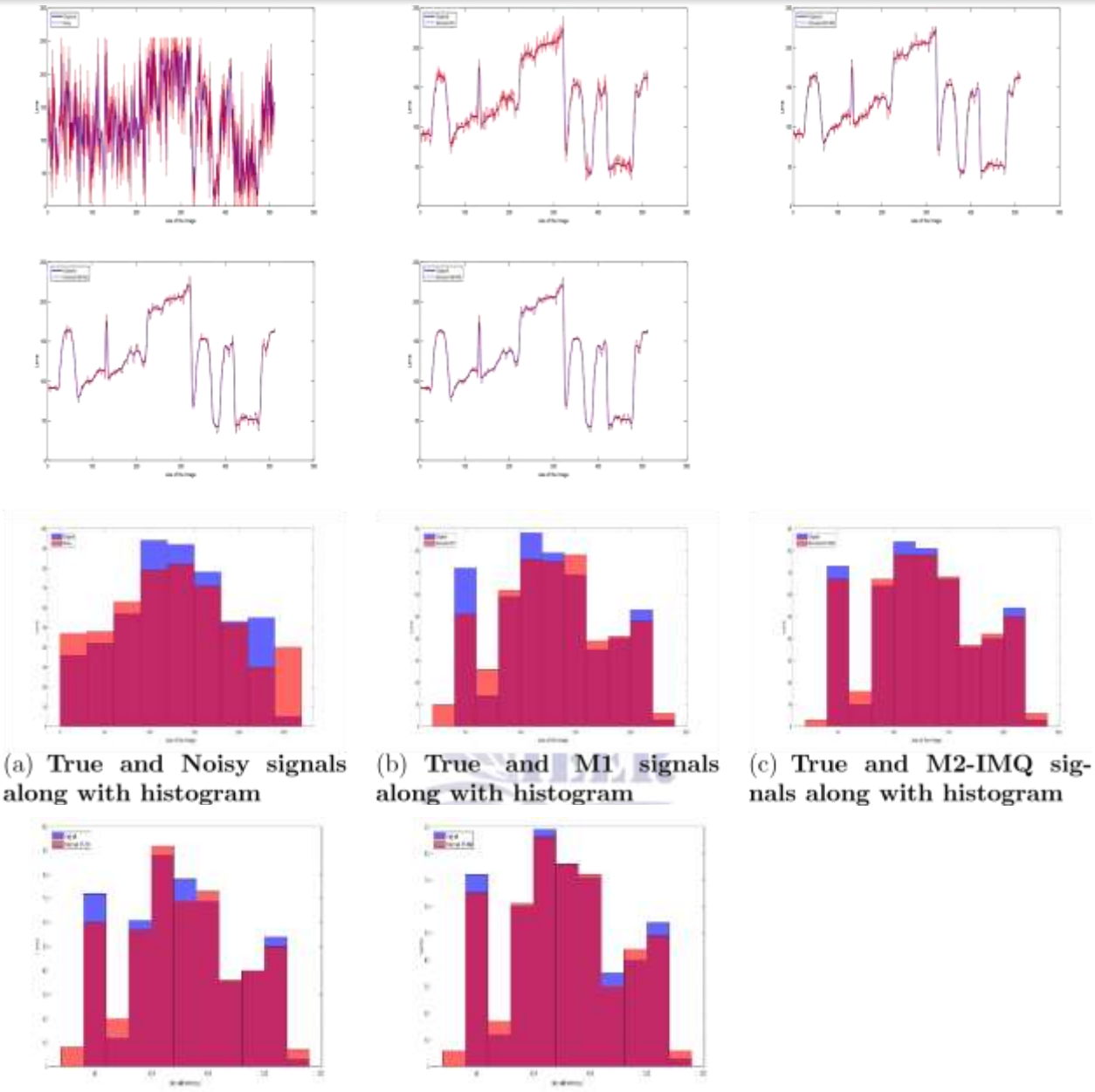

(a) True and Noisy signals along with histogram (b) True and M1 signals along with histogram (c) True and M2-IMQ signals along with histogram

(d) True and M2-GA signals (e) True and M2-MQ signals along with histogram

Figure 6: Comparison 110th signal taken from Lena image for signal denoising: (a) Ture and degraded signals with noise level is 50%; (b) Ture and denoised signals with histogram by M1; (c) Ture and denoised signals with histogram by M2 along with IMQ-RBF; (d) Ture and denoised signals with histogram by M2 along with GA-RBF; (e) Ture and denoised signals with histogram by M2 along with MQ-RBF. The actual signal is denoted by blue colour, while noisy and denoised signals are denoted by red colour.

Table 3: Comparison of SNR values of M1 and M2, which is connected with IMQ-RBF, GA-RBF, and MQ-RBF, respectively.

S.no	Signal selection of the Lena	Size	M1	M2(IMQ)	M2(GA)	M2(MQ)
			SNR	SNR	SNR	SNR
1	110^{th}	512^2	24.01	24.09	24.14	24.21

5. Concluding Remarks

This article has introduced the Local Meshless Collocation Algorithm (LMCA) for the numerical solution of the EL-PDE connected total Domain Decomposition method (DDM), and to get a smooth solution regarding signal de-noising with additive noise. The LMCA has the advantage of generating quick and better restoration performance (signal de-noising) due to its meshless nature, adaptive nature, MQ-RBF used as a basis function, and computational efficiency. The associated meshless scheme is checked on various signals and compared their results with the traditional method. The experimental results have revealed that the proposed meshless method (LMCM) is far better in signal restoration, i.e., signal de-noising (SNR values) and CPU time, compared with some traditional methods.

REFERENCE

Li, Xiaowei, Lei Li, and Qiong-Hua Wang. "Wavelet-based iterative perfect reconstruction in computational integral imaging." JOSA A 35, no. 7 (2018): 1212-1220.

Satapathy, L. M., P. Das, A. Shatapathy, and A. K. Patel. "Bio-medical image denoising using wavelet transform." Int. J. Recent Technol. Eng 8, no. 1 (2019): 2874-2879.

Naveed, Khuram, Bisma Shaukat, Shoaib Ehsan, Klaus D. Mcdonald-Maier, and Naveed Ur Rehman. "Multiscale image denoising using goodness-of-fit test based on EDF statistics." PLoS One 14, no. 5 (2019): e0216197.

Kervrann, Charles. "An adaptive window approach for image smoothing and structures preserving." In Computer Vision-ECCV 2004: 8th European Conference on Computer Vision, Prague, Czech Republic, May 11-14, 2004. Proceedings, Part III 8, pp. 132-144. Springer Berlin Heidelberg, 2004.

Polzehl, Jörg, and Karsten Tabelow. "Adaptive smoothing of digital images: The R package adimpro." (2007).

Ramadhan, Afrah, Firas Mahmood, and Atilla Elci. "Image denoising by median filter in wavelet domain." arXiv preprint arXiv:1703.06499 (2017).

Luo,Liang, Zhi-qin Zhao, Xiao-ping Li,and Xiang-chu Feng. "A stochastic image denoising method based on adaptive patch-size." Multidimensional Systems and Signal Processing 30 (2019): 705-725.

Liu,Feng, and Jingbo Liu. "Anisotropic diffusion for image denoising based on diffusion tensors." Journal of Visual Communication and Image Representation 23, no. 3 (2012): 516-521.

Bai,Jian, and Xiang-Chu Feng. "Image denoising using generalized anisotropic diffusion." Journal of Mathematical Imaging and Vision 60 (2018): 994-1007.

Chan,T., Esedoglu, S., Park, F. & Yip, A.(2006). Total variation image restoration: Overview and recent development.

Rudin,L.I., Osher, S., & Fatemi,E.(1992). Nonlinear total variation based noise removal algorithms. Physica D: Nonlinear Phenomena, 60(1–4),259–268.

Osher, S., Burger, M.,Goldfarb, D., Xu, J., & Yin, W. (2005). An iterative regularization method for total variation-based image restoration. Multiscale Modeling & Simulation, 4(2), 460–489.

Chang, Q., Chern, I. L., & McLaughlin, D. (2009). Total variation regularization for image restoration. Journal of Scientific Computing, 39, 20–45.

Lysaker, M., Lundervold, A., & Tai, X. C. (2004). Noise removal using fourth-order partial differential equations. IEEE Transactions on Image Processing, 12(12), 1579–1590.
Clason, C., Jin, B., & Kunisch, K. (2010). A duality-based splitting method for total variation image restoration. SIAM Journal on Scientific Computing, 32(3), 1484–1505.
Rudin, L. I., Osher, S., & Fatemi, E. (1992). Nonlinear total variation based noise removal algorithms. Physica D: Nonlinear Phenomena, 60(1–4), 259–268.
Osher, S., Burger, M., Goldfarb, D., Xu, J., & Yin, W. (2005). An iterative regularization method for total variation-based image restoration. Multiscale Modeling & Simulation, 4(2), 460–489.
Tikhonov, A. N., & Arsenin, V. Y. (1977). Solutions of Ill-Posed Problems. Wiley.
Makovetskii, Artyom, Sergei Voronin, and Vitaly Kober. "A generalized Condat's algorithm of 1D total variation regularization." In Applications of Digital Image Processing XL, vol. 10396, pp. 523-530. SPIE, 2017.
Makovetskii, Artyom, Sergei Voronin, and Vitaly Kober. "A generalized Condat's algorithm of 1D total variation regularization." In Applications of Digital Image Processing XL, vol. 10396, pp. 523-530. SPIE, 2017.
Aubert, Gilles, Pierre Kornprobst, and Giles Aubert. Mathematical problems in image processing: partial differential equations and the calculus of variations. Vol. 147. New York: Springer, 2006.
Rudin, L. I., Osher, S., & Fatemi, E. (1992). "Nonlinear Total Variation Based Noise Removal Algorithms." Physica D: Nonlinear Phenomena, 60(1-4), 259-268.
Wahba, G. (1990). Spline Models for Observational Data. SIAM.
Powell, M. J. D. (1987). Radial Basis Functions for Multivariable Interpolation. Advances in Numerical Analysis.
Fornberg, B., & Shane, H. (1988). Interpolation by Radial Basis Functions. Journal of Computational and Applied Mathematics.
D. D. Lee, & H. S. Seung. (2001). Algorithms for Non-negative Matrix Factorization. Advances in Neural Information Processing Systems.
Toselli, A., & Widlund, O. (2005). Domain Decomposition Methods—Algorithms and Theory. Springer.
Buhmann, M. D. (2003). "Radial Basis Functions." Acta Numerica, 9, 1-38.
Li, H., Zhang, H., & Wang, S. (2010). "A Domain Decomposition Method for the Solution of Partial Differential Equations." Journal of Computational Physics, 229(4), 1264-1282.
Hwang, S. W., Lee, Y. S., & Kim, H. J. (2011). "Local Radial Basis Function Method for the Numerical Solution of PDEs." Applied Numerical Mathematics, 61(12), 1342-1355.
Chung, S. J., Park, H. J., & Lee, C. (2004). "Parallel Domain Decomposition Methods for Meshless Radial Basis Functions." Computers & Mathematics with Applications, 47(10), 1521-1530.
Jiang, Y., Zhang, W., & Li, D. (2016). "Application of Local RBF Method in Fluid Dynamics." Computational Mechanics, 58(5), 915-929.
Widlund, O. (1999). "Domain Decomposition Methods for Partial Differential Equations." Numerical Mathematics, 84(3), 557-592.
Sajavičius, S.N., 2013. Optimization, conditioning and accuracy of radial basis function method for partial differential equations with nonlocal boundary conditions—A case of two-dimensional Poisson equation. Engineering Analysis with Boundary Elements, 37(4), pp.788-804.
Kansa, E. J. (1990). Multiquadrics—A scattered data approximation scheme with applications to computational fluid dynamics I: Solutions to parabolic, hyperbolic, and elliptic partial differential equations. Computers and Maths & Applics., 19, 147–161.